World Conference on Timber Engineering Oslo 2023

NUMERICAL ANALYSIS ON THE FLEXURAL PERFORMANCE OF COMPOSITE STEEL-TIMBER BEAMS UNDER FIRE CONDITIONS

Zhiyuan Liu[1,2], Binsheng Zhang[1,*], Huijuan Jia[2] and Tony Kilpatrick[1]

ABSTRACT: Recently, a novel type of composite structure, composite steel-timber (CST) structure, has attracted much attention by connecting steel and timber in an effective way to form composite structural components. However, the relevant research is lacking, especially in structural fire design and analysis. In this study, based on the sequentially coupled method, commercial finite element software ABAQUS was used to numerically simulate the dynamic performances in the temperature field and the flexural behaviours in the displacement field of a novel CST beam with steel element embedded within the Glulam and connected by adhesives and bolts under standard fire for two hours. During the numerical simulations, the temperature distributions within the CST beam were explored, and the flexural performances of the beam in the displacement field were examined. Through the comparative analysis, the temperature distributions of the embedded steel beam and the surrounding Glulam beam under one-hour standard fire verified the advantages of this type of CST beam in structural fire design. Parametric studies on the fire resistance of the CST beam were also conducted by adjusting the bolt spacing and the protection thickness of Glulam. The obtained results indicated that reducing the bolt spacing and thickness of the Glulam protection layer would have an adverse effect on the temperature distributions in the embedded steel element to a large extent.

KEYWORDS: composite steel-timber (CST) structure; structural fire design and analysis; numerical simulation and analysis; bearing capacity; refractory limit

1 INTRODUCTION

Since enhanced structural effectiveness and combined material properties, composite structures, especially composite concrete-steel structures have been thoroughly researched and form relatively complete structural systems. Recently, composite steel-timber (CST) structures have attracted more attention from researchers and gained initial engineering applications in Japan [1,2]. This innovative composition mainly combines advantages of high strength and excellent ductility of steel and decent sustainability and fire resistance of timber while potentially helping overcome the instability and fire susceptibility of steel members and brittle behaviour of timber components [3-6].

Based on the literature review, it is found that current researches are focusing on the structural performance, bearing capacity, initial stiffness and failure modes of various CST structural components, i.e. beams [7-9], columns [10-13], shear walls [14], flooring systems [15] and their connections [16,17] under static or cyclic loading conditions by experiments and/or numerical simulations and parametric studies to investigate the potential impacts brought by the adjustment of steel/ timber members' geometry and shear connectors' spacing on their ultimate load-bearing capacity. However, there are few investigations and analyses related to structural fire design and analysis of the CST structure.

Considering potential structural and economic losses brought by fire accidents in buildings, therefore, during structural design, fire safety has been regarded as a basic requirement and should be equally treated as the load carrying capacities [18]. Two methods are recommended for structural fire design and analysis based on Eurocodes. In practice, prescriptive approach is one of the commonly approaches recommended by Eurocodes and can be further divided into two categories, i.e. standard fire test method and simplified calculation method. Both methods for timber and steel materials are described in Parts 1-2 of Eurocodes 3 and 5 in details [19,20].

In this study, comprehensive numerical simulations were conducted by using ABAQUS to investigate the flexural performances and fire resistances of a novel CST beam under fire conditions with different bolt connection spacings and timber protection thicknesses by following general approaches indicated in Eurocodes 3 and 5.

2 PROFILES OF THE CST, GLULAM AND STEEL BEAMS

CST beams for simulations in this study were assumed to be used in Canada, where the annual average temperature

[1,2] Zhiyuan Liu, Glasgow Caledonian University (GCU), Glasgow, Scotland, UK & Jinling Institute of Technology (JIT), Nanjing, Jiangsu, China, ZLIU206@caledonian.ac.uk
[1*] Binsheng Zhang, Glasgow Caledonian University (GCU), Glasgow, UK, Ben.Zhang@gcu.ac.uk
[2] Huijuan Jia, Jinling Institute of Technology (JIT), Nanjing, Jiangsu, China, Jiahuijuan@jit.edu.cn
[1] Tony Kilpatrick, Glasgow Caledonian University (GCU), Glasgow, UK, A.R.Kilpatrick@gcu.ac.uk

https://doi.org/10.52202/069179-0229

is relatively low. Thus, the ambient temperature could reach 0℃. In addition, the composite beam could be integrated with timber or concrete floor slabs to form composite flooring systems and hence the CST beam could be seen as three sides directly exposed to fire in the structural fire analysis [21]. For simplification, each type of beam specimens was modelled and analysed for a unit length.

2.1 STANDARD CST BEAM

In Figure 1, the proposed standard CST beam was mainly composed of three parts: Glulam beam, steel beam and bolts. The Glulam beam was assumed to be formed by bonding ten Glulam blocks made of Canadian beech [22] with epoxy ethane adhesives. The steel beam was the steel I-beam section, with the dimensions of length × height × width × flange thickness × web thickness = 1000 mm × 150 mm × 100 mm × 8 mm × 6 mm, embedded in the middle of the Glulam beam with adhesives, and the outer edges of the steel beam flanges had a 50 mm distance to the outer edges of the Glulam beam. Common M20 bolts were selected to strengthen the composition, and the bolts had a 200 mm spacing in the longitudinal direction and penetrated into the composite beam.

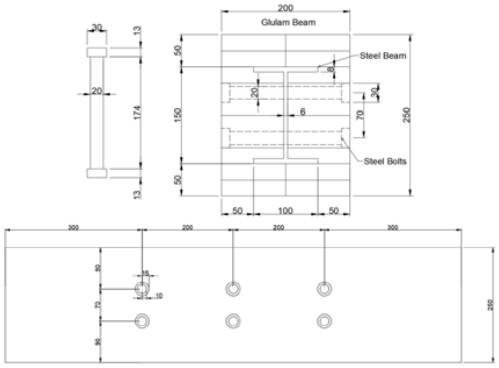

Figure 1: *Profiles of the CST beam model and M20 steel bolts for the standard CST beam*

2.2 COMPARED GLULAM AND STEEL BEAMS

As indicated in Figure 1, the Glulam and steel beams for comparison had the same sizes as the standard CST beam.

2.3 CST BEAMS FOR PARAMETRIC STUDY

As to the CST beams for the parametric study, illustrated in Figure 2, the bolt spacing was reduced from 200 mm to 150 mm or the protection thicknesses of the outer Glulam layer for the steel beam along the height and width were reduced from the original 50 mm to 30 mm.

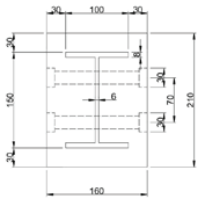

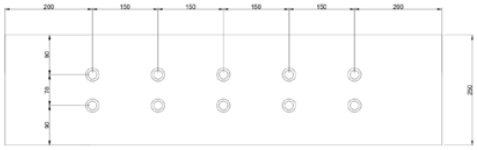

Figure 2: *The profiles of the parametric CST beam models*

3 FINITE ELEMENT ANALYSIS (FEA)

From the experimental test results, Tsai [13] and Zhang [26] indicated that the CST specimens did not have large structural deformations and damages that affected the heat transfer and temperature field distributions in the process of fire. Considering the accuracy in the thermal-solid coupling simulations and analyses on this kind of CST beam model and computational costs, the commercial finite element software ABAQUS and the sequentially coupled analysis method recommended by some previous researchers [26,27] was adopted.

Therefore, the temperature field would be first operated and analysed based on the ISO standard fire curve [28], and then the calculated temperature results were imported into the displacement field as the predefined field to calculate the final bending performances of the CST beams after being exposed to fire for 2 hours.

3.1 THE ESTIMATION METHOD

The material properties, including thermal and mechanical properties of steel and timber, show variations in response to elevated temperatures and their specific relationships would be input into ABAQUS in the tabular form based on the relevant specifications and the existing research data.

For steel, indicated by BS EN 1993-1-2 [19], its density ρ could be seen as a constant value when the surrounding temperature rises, i.e. ρ = 7850 kg/m^3, and the specific heat and thermal conductivity are shown as functions of temperature, respectively. Similarly, BS EN 1995-1-2 [20] also gives the suggested thermal parameter values for timber materials after fully considering water evaporation, wood carbonisation decomposition and material composition changes during combustion.

As for the mechanical properties, steel was regarded as an isotropic material and an elastic-linear – perfectly plastic model was adopted [27]. Generally, timber materials for Glulam have different properties in normal, radial and tangential directions and can be regarded as an ideal anisotropic elastoplastic body with suggested engineering data [22] for simulations.

3.2 SETUP OF THE NUMERICAL MODELS

During the modelling, the influence of adhesives on the temperature field was not considered. It was assumed that there was no air layer between the components. Because the thickness of the adhesives layer was small, and the heat from the external fire site would be quickly transferred to the interior components. The 3 mm fine mesh around the bolt holes and the 15 mm loose mesh for other areas were applied according to the configuration

https://doi.org/10.52202/069179-0229

characteristics of the parts. The final assembled model is shown in Figure 3.

Transient heat transfer and general static steps are defined for the thermal and mechanical models, respectively. Besides, the external fire site should be applied in the temperature field by defining an amplitude based on the standard fire curve, and in the displacement, the uniformly distributed load should also be directly applied on the top surface of the composite beam in the pressure form of 100 kN/m^2. As to the boundary conditions, the absolute zero temperature, the Steve-Boltzmann constant (5.678×10^{-8} W/m^{2}K^4) and the ambient temperature, the emissivity values (0.7 and 0.8 for steel and timber) and convection coefficient (25 W/m^2°C) [27] should be defined in advance to facilitate the calculations and analyses of heat conduction, radiation and convection in the temperature field. As to the contact definitions, in the normal direction, hard contact was defined to apply no restrictions to the pressures transferred between timber and steel and the Coulomb's friction model [26] with the friction coefficients of 0.3 and 0.001 for steel-timber and steel-steel contacts. During the flexural performance analysis, both ends of the composite beam in two directions shall be restricted, for the simulation requirement of a simply supported beam. More modelling details can be found from the ABAQUS User Manual [24].

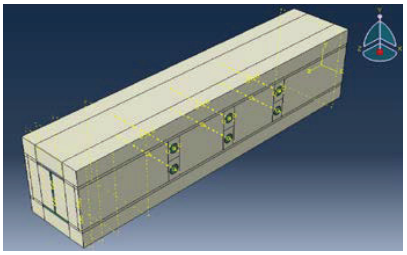

Figure 3: *The final assembled CST beam model in ABAQUS*

4 NUMERICAL SIMULATION RESULTS AND ANALYSES

4.1 TEMPERATURE FIELD ANALYSES

4.1.1 Temperature distributions

As shown in Figure 4, the temperature distributions for the Glulam, steel beam and steel bolts are presented and analysed.

The Glulam serving as the protection layer, firstly carried out heat transfer between itself and the surrounding fire environment. Therefore, the calculated node temperatures of the outermost layer of the Glulam quickly reached a high value, up to 1000°C, while the top surface of the Glulam beam was not directly affected because it directly contacted with the floor slab. The overall temperature distribution presented a trend that node temperatures would decline from the outside towards the centre, where they had the lowest values, which is consistent with the test results in the literature [26].

The web and lower flange of the steel beam were the parts with the highest temperatures in the whole beam, namely 350°C ~ 420°C. The bolt holes in the middle of the web, where steel bolts were through the beam and carried out the heat transferred from the external fire field, induced the rises in the node temperatures near the bolt holes of the steel webs, especially around the bolt holes near the bottom of the CST beam, which bear the double heat penetration from all three heat transfer directions of the fire field and from the external bolts. The upper flange at both ends of the steel beam was far away from the thermal penetration of the bolt holes and was insulated by the outer Glulam beam. Therefore, the node temperature did not increase significantly and remained at around 150°C.

All six bolts show the characteristics of high temperatures at both ends and lower temperatures in the middle. The reason for this is that both heads and nuts of the bolts were exposed first to fire conditions, and were surrounded by the Glulam beam, so the heat would mainly extend along the bolt direction, which was in line with the engineering practice. Furthermore, the temperature distributions of the lower bolts were slightly different from the upper ones and more unfavourable, which were consistent with the differences in the temperature distributions of the bolt hole areas adjacent to the lower and upper flanges of the steel beam, due to the uneven heat transfer from the fire field onto three sides of the CST beam. However, the temperatures of the central bolts at the mid-span were higher than those of the bolts near the supports, which may be due to the superposition effect of the temperature penetrations from the bolts on the left and right sides.

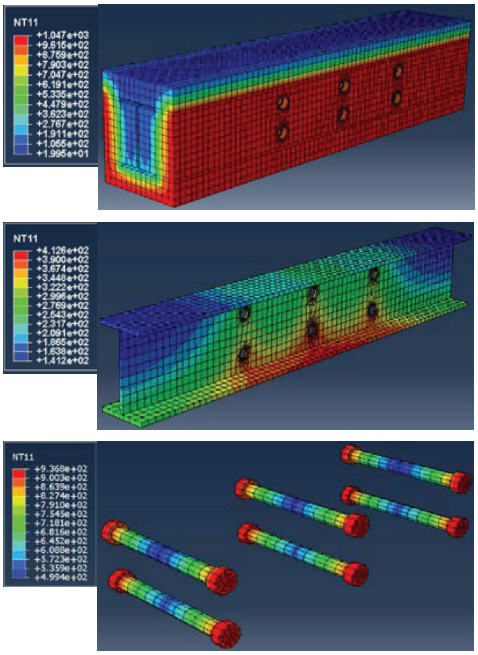

Figure 4: *Node temperature contours of the Glulam beam, steel beam and steel bolts at t = 120 min*

4.1.2 Assessment of the protection ability of Glulam

In Figures 5 and 6, the temperature distribution results at t = 15 and 60 min are presented and further analysed, combined with results illustrated in Figure 4, in terms of the protection effects brought by the external Glulam beam.

When *t* is equal to 15 min, according to the standard fire curve, the ambient temperature had completed nearly 70% of the final temperature loading, and the heads and nuts of the steel bolts had reached around 260°C. However, the overall temperature of the steel beam was no higher than 30°C because the outer Glulam beam provided good insulation, which was highly consistent with the Tsai's test results [13], and the protection effect of the outer Glulam was reliable and effective within the first 15 minutes under the fire conditions. In addition, due to the heat conduction of the bolts through the CST beam, the temperature growth of the steel beam started from the bolt holes in the steel web and gradually extended to the flanges and both ends of the steel beam.

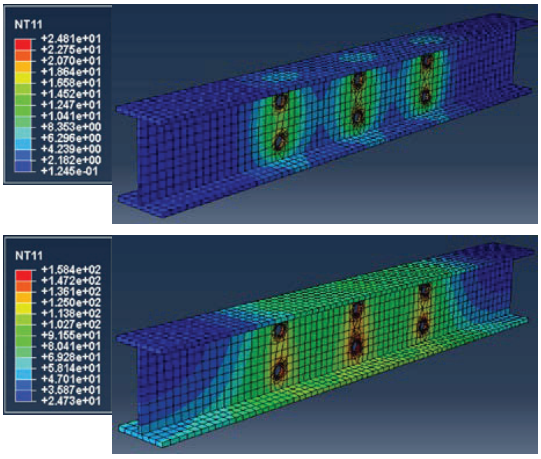

Figure 5: *Node temperature contours of the steel beam at t = 15 min and 60 min.*

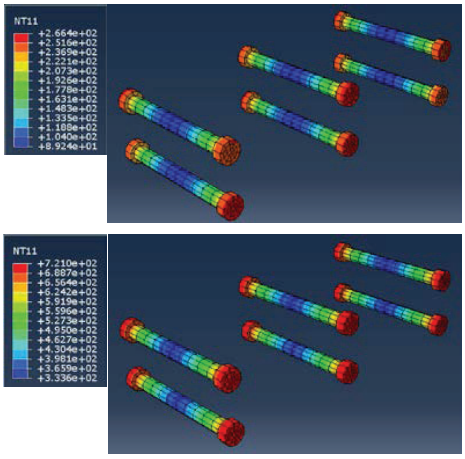

Figure 6: *Node temperature contours of the steel bolts at t = 15 min and 60 min.*

When the standard fire was applied for 60 minutes, the ambient temperature gradually increased to 945.3°C. At this point, the temperature field near the areas of the bolt holes in the middle of the steel beam became significantly superposed, and the temperatures in the areas at the mid-span were the highest, which was presented by the software with the large red block. In addition, the mid-span temperature "diffusion" increased further and extended to the lower flanges at both ends of the beam, but the temperatures in the upper flanges at both ends remained below 50°C. Combined with the temperature field distributions of the bolts at this time, the node temperatures in the middle of the bolts had reached the temperature range of 330°C ~ 400°C, while the maximum temperature in the middle of the steel beam was only about 160°C, presenting a "gap" of heat transfer. This may be because when the bolts temperature rose rapidly, part of the heat was absorbed by the surrounding Glulam beam, while the rest was absorbed by the steel beam. In other words, the internal Glulam played a vital role in absorbing and blocking the fire heat transferred from the bolts.

After the 2-hour burning, the temperature increment of the external fire site levelled off, reaching 1049°C, and the heat transfer lasted for quite a long time. However, from Figure 5, the highest temperature zone of the steel beam occurred in the web and lower flange of the mid-span, reaching about 410°C, while the temperatures in most areas were in the range of 200°C ~ 300°C. This distribution characteristic was similar to that in the 60-minute stage where the temperatures at both ends were low and those at the mid-span were high. According to the typical stress-strain curves [29] of the steel (see Figure 7) at elevated temperatures, the mid-span of the inner steel beam could retain most of its yield strength, and more strains could be spared for deformations, showing stronger plasticity even in the 120-minute fire stage.

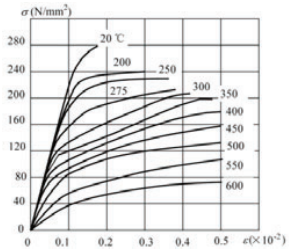

Figure 7: *Typical stress-strain curves of steel at elevated temperatures [29].*

4.1.3 Analysis of the charring results of the Glulam

For the ABAQUS simulations, the timber elements with temperatures exceeding 300°C should be regarded as the carbonised layers. Charring rate, referring to the ratio of the depth of the charring layer to the fire exposure time, is an important index to verify the accuracy of the numerical model. However, the charring rate is not constant [26], and the formation of the charring layer hinders the heat transfer to the interior. Therefore, with the increase of the heating time, the charring rate decreases.

The charring depths and charring rates were roughly calculated (based on the bottom surface) by analysing the temperature distributions in the CST beam section in four time points (see Table 1). According to the calculated data in the table, it can be found that the charring depth increased with the increase of the acting duration of the standard fire curve, while the charring rate decreased as the process continued, which would basically conform to

https://doi.org/10.52202/069179-0229

the law mentioned above. Besides, with the increase of the charring depth, the outer Glulam gradually lost its ability to protect the steel, and Figure 8 shows that a 50 mm outer Glulam protection layer for the steel beam was basically burned out completely. If the fire temperature kept rising, the temperatures in the steel beam would quickly increase, eventually causing the complete strength loss of the steel.

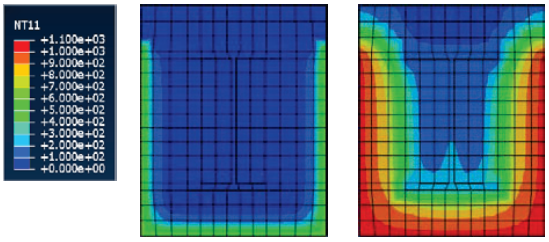

Figure 8: *Temperature field distributions of the CST beam section at t = 15 min and 120 min.*

Table 1: *Summary of the charring depth and rate results at the selected four time points*

Time duration (min)	Charring depth (mm)	Charring rate (mm/min)
15	13.3	0.89
30	20.2	0.67
60	30.1	0.50
120	49.8	0.42

4.2 DISPLACEMENT FIELD ANALYSES

4.2.1 Analysis of the simulation results

Figure 9 illustrates the 3D displacement and von Mises stress contours of the embedded steel beam. For the simulated displacement results, the maximum displacement appeared in the mid-span region and decreased from that region toward both ends. This was consistent with the displacement distribution of a simply supported steel beam under bending actions at room temperature. Under the uniformly distributed load of 100 kN/m^2, i.e. 10 kN/m line load, the maximum displacement was 9.65 × 10^{-5} m. According to the linear relationship between the maximum mid-span displacement and bending loads applied onto the steel beam, combined with the generally recognised deflection limit of L/360 under service loading, the maximum load capacity could be estimated to be close to 300 kN/m, which also matches the engineering practice. Therefore, this served as an initial validation for the established model and based on this, reflected a good deformation capacity for the embedded steel beam subjected to the 2-hour fire conditions.

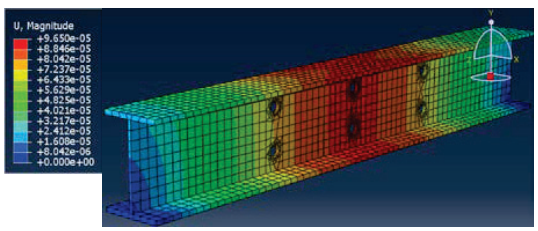

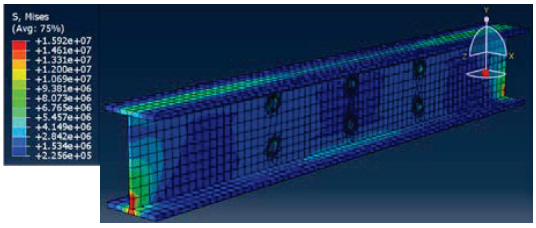

Figure 9: *Simulated 3D displacement and von Mises stress of the embedded steel beam in the displacement field.*

The 3D von Mises stress contour shows that lower flange at the two ends and the upper flange in the middle span region of the steel beam sustained unfavourable stress distributions. This may be because the steel beam at this moment had a tendency of buckling on both sides of the upper flange under the applied uniformly distributed load, and the lower flange in the middle span, subjected to the highest bending moment and tensile stress, was weakened by the bolt holes in the web, resulting in strong stress concentrations. The general trends matched the original expectations and were similar to the generally recognised stress distributions of the steel beam under the bending action. However, due to the restrictions of the outer residual timber beam, the stress distributions of the embedded steel beam were not obvious.

4.2.2 Manual estimation calculations

Figure 10 illustrates the simplified calculation diagram of the steel beam and the geometrical parameters of its cross-section by ignoring the imperfection effect caused by the bolt holes in the steel web. Therefore, the second moment of area and the sectional modulus of the steel beam could be calculated as 9277185 mm^4 and 123696 mm^3. It was also assumed that the UDL acting on the steel beam was w in kN/m, including the self-weight of the steel beam and the variable loads on the upper flange.

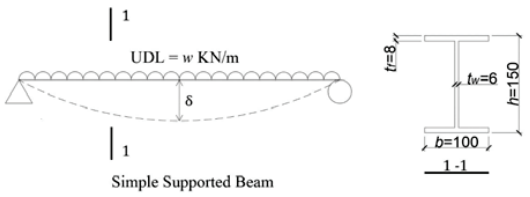

Figure 10: *Illustration of the simply supported embedded steel beam under the UDL.*

Under fire conditions, the maximum temperature of the embedded steel appeared in the lower flange at the mid-span, which coincided with the maximum bending moment and deflection point of the steel beam under the static loading at room temperature. In this case, the load bearing capacity calculation would mainly be focused on the mid-span location. The temperature at the mid-span of the steel beam reached 416°C after a two-hour standard fire. According to BS EN 1993-1-2 [19], both the elastic modulus and yield strength of steel would drop at this temperature and the reduction coefficients could be applied as 0.685 and 0.97, respectively, i.e. E = 0.685 ×

210000 = 143850 N/mm^2 and f_y = 0.97 × 400 = 388 N/mm^2.
According to BS EN 1993-1-1 [30], the bending moment capacity could be related to the UDL as

$$M_{c,Rd} = \frac{W_{pl} f_y}{\gamma_{M0}} = \frac{123695.80 \times 388 \times 10^{-6}}{1.0} = M_{Ed} = \frac{w L^2}{8}$$

i.e. $M_{c,Rd}$ = 47.99 kNm and w = 383.95 kN/m.
Under the UDL w = 383.95 kN/m, the mid-span deflection δ_{max} would be:

$$\delta_{max} = \frac{5 w L^4}{384 E I} = 3.75 \text{ mm} > \delta_{limit} = \frac{L}{360} = 2.78 \text{ mm}$$

The steel beam failed due to the exceeded deflection under the UDL w = 383.95 kN/m. Thus, letting the maximum deflection at the mid-span be equal to its limit would yield the maximum UDL the steel beam could support, that is, w = 284.70 N/mm = 284.70 kN/m.
At this time, although the bearing capacity could reach up to 383.95 kN/m, the deflection would exceed its design limit. Therefore, if the deflection requirements were met, the final bearing capacity would still need to be further reduced. However, in practice, since the outer Glulam beam had not completely burned out, it serves as a T-shape coating outside the steel beam to limit its excessive deflection and the buckling failure of its upper flange and web. Thus, the ultimate bearing capacity would still be governed by the bending moment capacity.

4.3 COMPARATIVE ANALYSES

4.3.1 Steel Beam

A steel beam model with the same size as the embedded steel section in the standard CST beam was created in ABAQUS (without bolt holes), with the similar step, amplitudes and interactions assigned as well. The calculation results for t = 15 min were selected and are shown in Figure 11 below.
It can be seen from the figure that, without the protection of the outer Glulam, the temperature of the steel beam rapidly reached above 600°C within only 15 min, and the highest temperature in the web was nearly 700°C. The steel beam exhibited "thermo-plastic" phenomenon, and most of the strength was lost. At this moment, even a small load was applied on the steel beam, its web would quickly buckle due to insufficient strength and stiffness, leading to the failure of the steel beam.

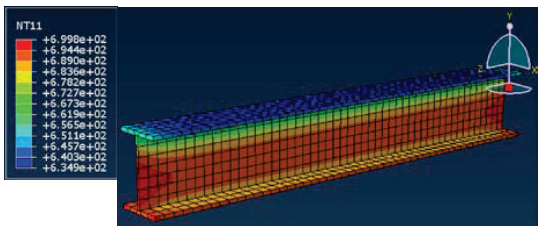

Figure 11: *Node temperature contour of the pure steel beam at t = 15 min.*

4.3.2 Glulam beam

The Glulam beam model without embedded steel and through bolts was created in ABAQUS with the same size as the external Glulam beam of the standard CST at t = 15 min and 60 min.
It is apparent that the overall temperature distributions and charring depth of the Glulam beam, which was about 16.7 mm, were similar to those of the CST beam. This means that the steel bolts, which brought the heat from the outside fire environment, did not have a critical effect on the overall temperature distributions of the Glulam beam during the first heating hour. As for its bending capacity, it could be estimated by using the reduced cross-section method, as described in BS EN 1995-1-2 [20]. In this case, the effective cross-sectional dimensions of the Glulam beam were smaller than 160 mm × 230 mm under the external loads. However, with the introduction of the steel beam, the overall bearing capacity can be a sum of the individual capacities of both Glulam and steel beams [13], which was greatly improved. Moreover, with the increase of the fire exposure time to one hour, the external Glulam gradually lost most of its strength, with the charring depth to 45.2 mm, while the steel beam material strength reduction was relatively small. Thus, the overall combined value would still show a good bearing capacity or resistance to the external loads.

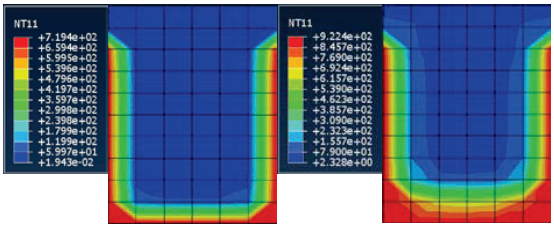

Figure 12: *Temperature distribution contours of the pure Glulam beam section at t =15 min and 60 min.*

5 PARAMETRIC STUDY

To improve the simulation efficiency in ABAQUS, parametric models were symmetrically established as the quarter of an entire beam by creating appropriate symmetry boundary conditions in ABAQUS.

5.1 EFFECT OF REDUCING BOLT SPACING

5.1.1 Charring characteristics

The charring depth was basically the same as that of the standard beam without significant difference for up to one-hour fire exposure (see Figure 13). However, when the fire action extended to 2 hours, the node temperatures of the bottom of the Glulam beam reached 400°C, and thus it was considered that all the protection layers of Glulam failed by then.

5.1.2 Temperature field of the embedded steel beam

By comparing Figures 4 and 14, it can be found that in terms of the overall temperature distributions, due to the decrease in the bolt spacing, more heat from the external fire field penetrated into the internal steel beam through the bolts, specifically through the bolt hole areas in the

https://doi.org/10.52202/069179-0229

web, which resulted in the heat conduction to the surrounding area and eventually the overall temperature distributions in the steel. For instance, for t = 60 min, the average temperature in the steel web exceeded 130°C, while the average temperature in the standard beam was only 110°C. In addition, the smaller bolt spacing made it easier to connect and superimpose the temperature fields around adjacent bolt holes. This could be verified by the fact that the temperature field near the areas of the bolt holes of the standard beam for t = 15 min only had a tendency, while the current beam model completed most of the temperature field connections. Consequently, due to this strengthened superimposition impact, after burning in the fire field for 120 min, the lower flange of the embedded steel beam had reached 462°C. Compared with that of the standard CST beam, namely 416°C, the temperature rose significantly.

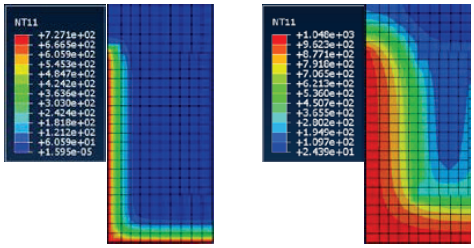

Figure 13: *Node temperature contours of the Glulam section of an adjusted CST beam with the reduced bolt spacing at t = 15 min and 120 min.*

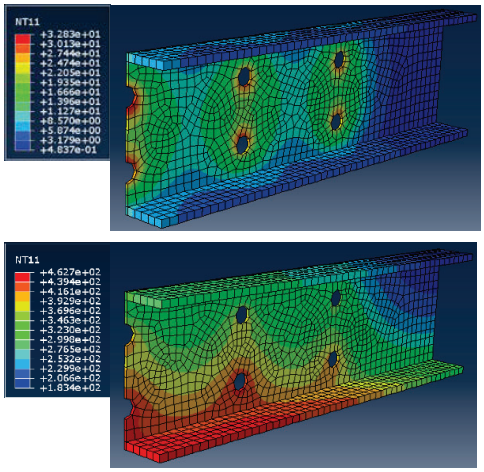

Figure 14: *Temperature contours of the quarter steel beam with the reduced bolt spacing at t = 15 min and 120 min.*

5.1.3 Estimated consequent displacement field

The reduction in the bolt spacing and the increase in the number of bolts per unit length could improve the composition robustness of the Glulam and steel beams, and additionally better the bending performances under room temperature. For structural fire design and analysis, this adjustment would pump more external heat into the internal steel beam, making the temperatures in its web rise faster. Especially after the structure was exposed to the fire for 2 hours, the Glulam at this moment was completely burnt out, and the lower flange of the embedded steel beam would be fully exposed to the fire. If a continuous fire field was applied, the steel beam would be heated up quickly and largely lose its strength. In other words, this would finally weaken the protection ability of Glulam, and the steel beam would lose its bearing capacity faster than the standard CST beam.

5.2 EFFECT OF REDUCING GLULAM PROTECTION THICKNESS

5.2.1 Charring characteristics

By comparing Figures 8 and 15, it can be found that there was a big difference in the charring depth of the adjusted model at t = 2 hour, but there was not much difference between the corresponding charring depths at t = 15 min. This could be because when the protection layer thickness of the Glulam decreased with the increase of the fire duration, the protection layer was burned off and heat gradually came into contact with the bottom flange of the steel beam. Thus, the steel beam could well transfer the heat evenly to other areas of the beam for a better thermal conductivity. This would help absorb some heat from the Glulam. When the action time was small, the protection effect of Glulam still played a governing role, and thus the charring depth difference was not so big.

5.2.2 Temperature field of the embedded steel beam

By comparing Figures 5 and 16, it can be found that because of the reduced protection layer thickness of the Glulam, heat from the fire environment would be able to penetrate the bottom flange of the embedded steel beam more quickly, and this led to the quicker rises in the overall temperatures in the steel beam. Especially, at t = 60 min, the average temperature of the lower flange had exceeded 230°C, while the average temperature of the standard beam was only 120°C. This huge difference became more obvious in the 120-min temperature field. At this moment, the maximum node temperature occurred at the mid-span of the lower flange and reached almost 670°C, which was much higher than that of the standard CST beam model, namely 416°C, and would cause excessive reductions in the material properties. Hence, reducing the thickness of the Glulam protection layer would greatly increase the heating rate of the embedded steel beam.

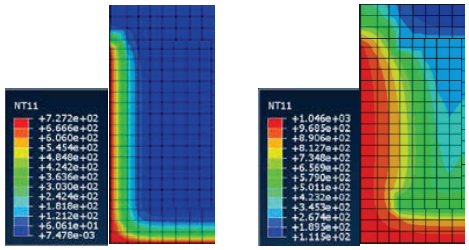

Figure 15: *Node temperature contours of the Glulam section of an adjusted CST beam with the reduced Glulam protection layer at t = 15 min and 120 min.*

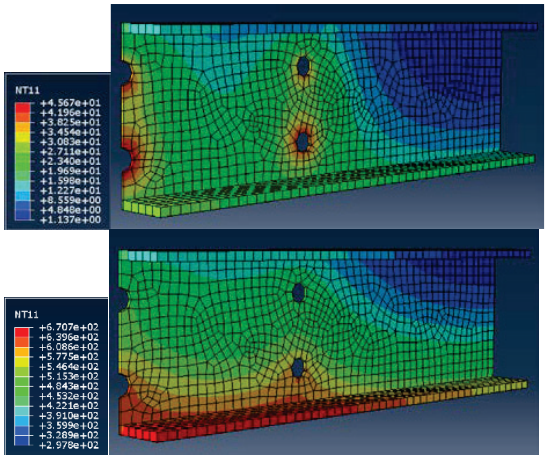

Figure 16: *Node temperature contours of the quarter steel beam with the reduced Glulam protection thickness at t = 15 min and 120 min.*

5.2.3 Estimated consequent displacement field

Although the thickness of the protection layer of the Glulam is reduced, the self-weight of the composite beam decreases as well, and thus the structural efficiency under room temperature will be improved to a certain extent which eventually reduces the costs. However, in terms of structural fire design and analysis, such adjustment will make the heating rate of the embedded steel accelerate because its lower flange prematurely participates in the heat transfer of the temperature field of the whole structure, and the refractory limit will be greatly reduced. If the requirements of structural efficiency and fire resistance are considered at the same time, the optimal protection layer thickness can be determined through subsequent experiments and analysis for achieving the double benefits of economy and structural safety.

6 Conclusions

In this research, based on the commercial finite element analysis software ABAQUS, numerical simulations and analyses of the temperature field and displacement field of the standard CST beam were conducted in a sequential coupling way. Through the analyses on the temperature field results, the validity of the calculation model was verified, and the heat transfer process and distribution characteristics of this type of CST beam under fire conditions were summarised. By analysing the results of the displacement field, the flexural performances of the embedded steel beam after the fire were determined. Additionally, the corresponding steel beam and Glulam beam models were simulated for comparison, and the advantages of this type of CST beam in the structural fire design were verified. Finally, by adjusting the parameters of the standard CST beam model, the effects of reducing the bolt spacing and the Glulam protection layer thickness on the temperature fields of the CST beam were analysed, respectively.

Based on the obtained numerical results, the following conclusions on the research results can be drawn.

- After the 120-min standard fire, the 50 mm external Glulam protection layer was almost burned out and charred completely. However, this could effectively protect the embedded steel beam, except the areas of the bolt holes at the mid-span, from experiencing excessive temperature rises and help maintain most of its mechanical properties and structural performances.
- Under the uniformly distributed load, the embedded steel beam showed fairly good flexural resistance, and the stress and displacement distributions were not largely different from those at normal temperature.
- Pure steel beams and Glulam beams compared with the CST beams, presents the inferior loading bearing capacity due to the strength loss induced by “thermos-plasticity” or the excessively reduced effective cross-section area.
- Although reducing the bolt spacing, i.e. increasing the number of bolts per unit length, could improve the composition integrity of the two materials, but under fire conditions, it reversely promoted the temperature field superposition of the bolt hole areas in the steel beam web and accelerated the heating rate in the embedded steel beam, and thus the ultimate load bearing capacity and refractory limit could be reduced.
- Although reducing the thickness of the Glulam protection layer, i.e. reducing the self-weight of the CST beam, and improving the structural and economic efficiencies, the distributions of the composite structure in the temperature field were largely affected. After the 60-minute standard fire, the Glulam protection layer was completely burned out, and the continuous heating would lead to a rapid rise in the temperature in the embedded steel, and finally the overall failure of the composite steel-timber beam structure would happen.

In general, the structural fire analysis of the new type of CST beam, carried out through the numerical simulations in this study, was relatively abundant, after verifying its potential advantages in fire engineering, evaluating its flexural performance under the two-hour standard fire, and assessing the impacts of the variations in the bolt spacing and Glulam protection thickness on the structural performances of the CST beam under fire conditions. In the future, the comparative explorations between laboratory combustion data and numerical simulation results as well as the parameter optimisation analyses based on the secondary development of finite element software will be the focus of subsequent research.

ACKNOWLEDGEMENTS

This project is supported by both the School of Computing, Engineering and Built Environment at Glasgow Caledonian University, Scotland, UK, and the Department of Civil Engineering, School of Architectural Engineering, Jinling Institute of Technology, Jiangsu Province, China. The project is also supported by the MDPI journal Buildings, together with its Special Issues

https://doi.org/10.52202/069179-0229

"Advanced Concrete Structures in Civil Engineering" and "Dynamic Performances of Building Structures".

REFERENCES

[1] Fujita, M., Sakai, J., Oda, H. and Iwata, M. Building system for a composite steel-timber structure. *Steel Construction*, 2014, 7(3), 183-187.

[2] Japan Association of Building Construction Technicians (JABCT): 100 Selected Typical Examples of Structural Technology in Japan. China Building Industry Press, Beijing, China, 2005.

[3] Liu, Z., Jia, H., Wu, C., Li, M. and Chen, X. Research on the life cycle management method of 3D visualized fabricated steel structure based on BIM technology. In *Proceedings of Jiangsu Steel Structure Conference*, Oct 2019, Nanjing, China, 238-242.

[4] Zhang, Y. and Zhou, X: Design Principle of Steel Structure (2nd Ed). Higher Education Press, Beijing, China, 2004.

[5] Bai, R., Jiang, Z. Research on steel-timber composite structure. *Journal of Hebei Institute of Architecture and Civil Engineering*, 2016, 34(3), 75-78.

[6] Wang, X., Chen, Z., Bai, J., Li, S. and An, Q. Research status and development prospect of timber-steel composite structure. In *Proceedings of National Steel Structure Academic Annual Conference*, Apr 2011, Kunming, China.

[7] Chiniforush, A.A., Valipour, H., Akbarnezhad, A. and Bradford, M. Steel-timber composite (STC) beams: Numerical simulation of long-term behaviours. *Eurosteel*, 2017, 1(2-3), 2051-2059.

[8] Fujita, M. and Iwata, M. Bending test of the composite steel-timber beam. *Applied Mechanics and Material*, 2013, 351-352, 415-421.

[9] Luo, J., Li, Q. and Deng, R. Numerical analysis on flexural performance of a new kind timber-steel composite beams. *Low Temperature Architecture Technology*, 2017, 39, 46-48.

[10] Pan, F. *Experimental Research and Finite Element Analysis on Steel-Timber Combined Members*. Master's Thesis, Southeast University, Nanjing, China, 2008.

[11] Wang, J. and Duan, S. Experimental analysis of eccentric pressure behaviour of steel-timber composite columns. *Building Technology*, 2019, 46(9), 16-17.

[12] Hua, Q., Gao, Y., Meng, X. and Diao, Y. Axial compression of steel-timber composite column consisting of H-shaped steel and Glulam. *Engineering Structures*, 2020, 216, 1-12.

[13] Le, T. and Tsai, M. Behaviour of timber-steel composite with dowel connection under fire. *Key Engineering Materials*, 2019, 803, 195-199.

[14] Liu, Y., Chen, Z., An, Q. and Chen, B. Experimental investigation on lateral resistance performance of light timber-steel hybrid shear wall. *Journal of Tianjin University (Science and Technology)*, 2017, 50, 78-83.

[15] Zhou, X., Li, Z., Wang, R. and Shi, Y. Study on load-carrying capacity of the cold-formed steel joists-OSB composite floor. *China Civil Engineering Journal*, 2013, 46(9), 1-11.

[16] Keipour, N., Valipour, H.R. and Bradford, MA. Steel-timber composite beam-to-column joints: Effect of connections between timber slabs. *Journal of Constructional Steel Research*, 2018, 151, 132-145.

[17] Hassanieh, A., Valipour, H.R., Bradford, M.A. and Sandhaas, C. Modelling of steel-timber composite connections: Validation of finite element model and parametric study. *Engineering Structures*, 2017, 138, 35-49.

[18] Knobloch, M. Structural fire design - developments in research and assessment of fire in steel and composite structures. *Eurosteel*, 2017, 1(2), 133-142.

[19] BSI. *BS EN 1993-1-2:2005 Eurocode 3: Design of Steel Structures - Part 1-2: General Rules - Structural Fire Design*. The British Standards Institution (BSI), London, UK, 2005.

[20] BSI. *BS EN 1995-1-2:2004 Eurocode 5: Design of Timber Structures - Part 1- 2: General - Structural Fire Design*. The British Standards Institution (BSI), London, UK, 2004.

[21] Zhang, J., Liu, Z., Xu, Y., Ma, S. and Xu, Q. Experimental and numerical study on the charring rate of timber beams exposed to three-side fire. *Science China: Technological Sciences*, 2012, 55 (12), 3434-3444, 10.1007/s11431-012-4996-1.

[22] Product Guide: Glulam. Available online: https://www.apawood.org/publication-search?q=X440&tid=1 (Accessed on 10 November 2020).

[23] 3D EXPERIENCE, ABAQUS; Version 2020 [Computer software]; Dassault Systèmes Simulia Corp., Providence, RI, USA. 2019.

[24] ABAQUS 6.14: Analysis User's Guide. Available online: https://www.academia.edu/28334906/ Abaqus_Analysis_Users_Guide/ (accessed on 20 May 2021).

[25] Zhu, Y. and Cai, W. *Introduction to ABAQUS/ Standard Finite Element Software - ABAQUS/CAE Edition*. Tsinghua University Press, Beijing, China, 2003.

[26] Zhang, Y. *Experimental Study on the Fire Performance of Post-and-Beam Timber Structure with Bolted Steel-Timber Connection.* Master's Thesis, Southeast University, Nanjing, China, 2016.

[27] Ohene, A.A. *Modelling the Fire Performance of Hybrid Steel-Timber Connections*. Master's Thesis, Carleton University, Ottawa, Canada, 2014.

[28] ISO. *ISO 834-1: Fire Resistance Tests - Elements of Buildings Construction - Part-1: General Requirement*, International Organization for Standardization (ISO), Switzerland, 1999.

[29] Li, G. and Wang, W. State-of-the-art and development trend of fire safety research on steel structures. *China Civil Engineering Journal*, 2017, 50(12), 1-8.

[30] BSI. *BS EN 1993-1-1:2005 + A1:2014 Eurocode 3: Design of Steel Structures −Part 1-1: General Rules and Rules for Buildings*. The British Standards Institution (BSI), London, UK, 2005.